NASA/TM–2025–NASA/TM–2025–TBD

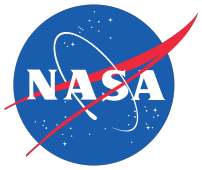

Acoustic Signatures of Incipient Boiling for Cryogenic Propellants: Part II—Machine-Learning–Based Detection and Characterization

Andrew Martinez
California Polytechnic State University, San Luis Obispo, California

James Lamkin
California Polytechnic State University, San Luis Obispo, California

Krishnanshu Gupta
California Polytechnic State University, San Luis Obispo, California

Zachary Weinfeld
California Polytechnic State University, San Luis Obispo, California

National Aeronautics and
Space Administration

Ames Research Center
Moffett Field, California 94035

July 2025

Acoustic Signatures of Incipient Boiling for Cryogenic Propellants: Part II—Machine-Learning–Based Detection and Characterization

Andrew Martinez
Statistics Dept.
Cal Poly, SLO
San Luis Obispo, CA
amart531@calpoly.edu

James Lamkin
Computer Science Dept.
Cal Poly, SLO
San Luis Obispo, CA
lamkin@calpoly.edu

Krishnanshu Gupta
Computer Science Dept.
Cal Poly, SLO
San Luis Obispo, CA
kgupta15@calpoly.edu

Zachary Weinfeld
Mathematics Dept.
Cal Poly, SLO
San Luis Obispo, CA
zweinfel@calpoly.edu

Summary

Understanding and detecting early-stage boiling in cryogenic fuel tanks is essential for maintaining the safety and stability of space missions. Traditional thermal sensing systems often lack the temporal sensitivity required to capture the onset of boiling phenomena, particularly under microgravity conditions where fluid dynamics differ significantly from terrestrial environments. This memorandum presents a machine learning framework that leverages acoustic emissions to characterize boiling behavior and detect incipient boiling phases prior to measurable pressure excursions. Using data from 441 cryogenic boiling experiments, time and frequency domain features were extracted from high-resolution accelerometer signals. These features informed the development of an unsupervised clustering pipeline for regime discovery and a supervised decision tree classifier for interpretable regime prediction. A custom web-based application was also developed to support real-time classification and exploratory data analysis. The resulting system enables non-intrusive, rapid, and feature-transparent assessment of boiling regimes and offers a potential enhancement to current cryogenic fuel monitoring methodologies.

1 Introduction

Cryogenic fuels are essential to modern spaceflight, providing high energy density and efficient propulsion. Storing these fuels safely is a complex challenge, particularly under microgravity conditions, where conventional convective cooling is reduced and localized heating can result in unstable boiling. In such environments, even minor heat leaks along the tank walls can superheat the fluid, initiating incipient boiling that rapidly generates vapor. This sudden transition can trigger pressure spikes severe enough to rupture the tank, endangering missions and equipment.

Current approaches to monitoring cryogenic tank stability rely heavily on thermal sensors. While effective at capturing temperature trends, these sensors are not well suited for detecting the earliest acoustic signatures of boiling, especially in dynamic microgravity environments. These sensors often provide delayed feedback, creating a possibility of pressure escalation without warning.

Boiling events are hypothesized to produce distinct acoustic signatures, detectable via accelerometers mounted on the tank exterior. The formation, growth, and collapse of vapor bubbles each emit energy that propagates through the tank walls and can be captured as sharp spikes in acoustic data. These patterns vary based on boiling regime, offering a promising nonintrusive signal for early detection.

This work builds on prior research in acoustic-based monitoring by combining signal processing with machine learning techniques. Unsupervised clustering is used to uncover latent boiling regimes, and a supervised decision tree classifier is trained to predict them based on interpretable signal features. A custom-built Dash web application supports both retrospective analysis and prospective classification, allowing exploration of trained model structures and real-time classification of new experimental data.

The resulting system enables rapid insight generation, interpretable modeling, and spatial analysis of boiling dynamics, with the goal of enhancing the safety and responsiveness of cryogenic fuel monitoring systems.

2 Dataset Description

This study utilizes data from 441 boiling experiments, each lasting between 1 and 30 seconds. The experiments were conducted using a cryogenic tank instrumented with acoustic sensors under controlled laboratory conditions.

2.1 Experimental Setup

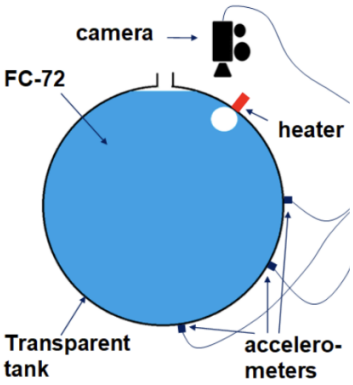

Figure 1.—Experimental setup: cryogenic tank with externally mounted accelerometers.

Each experiment consists of a spherical tank partially filled with liquid and equipped with accelerometers mounted on the tank walls, as illustrated in Figure 1. During each run, a localized heat source induces boiling near the wall surface, and acoustic emissions are recorded via the accelerometers. Although two sensor channels are available, the analysis presented here focuses on a single channel due to signal redundancy. The sampling rate for each sensor is 10,000 Hz.

2.2 Data Format and Visualization

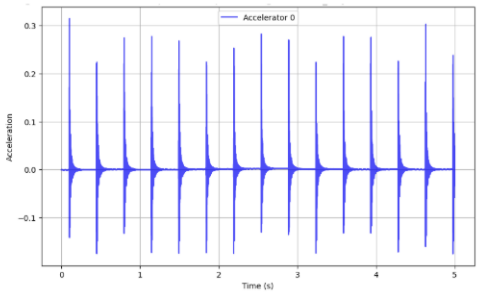

Figure 2.—Raw time-domain signal from a representative boiling experiment.

Each run is stored in a comma-separated values (CSV) file containing time-stamped accelerometer data. The raw time-domain signal is visualized in Figure 2 as amplitude versus time, where prominent peaks correspond to bubble nucleation and collapse events.

2.3 Physical Interpretation

Both time-domain and spectral analyses emphasize the acoustic signatures produced by vapor bubble nucleation and collapse during boiling. As superheated liquid approaches its boiling point near the heat source, vapor bubbles form and grow rapidly before collapsing or detaching. These transitions release localized energy in the form of pressure waves, which appear as sharp spikes in the acoustic signal. Distinct boiling regimes, such as quasi-homogeneous or heterogeneous nucleation, can generate characteristic patterns in the acoustic profile. Under microgravity conditions, convective heat transfer is significantly reduced, leading to more severe local superheating and more violent boiling behavior. These effects tend to manifest as particularly pronounced and structured acoustic features.

3 Feature Engineering

Features are extracted from both time and frequency domains to capture multiple dimensions of the boiling signal and enable characterization of different boiling regimes.

3.1 Time Domain Features

3.1.1 Peak Detection

SciPy's `find_peaks` is used with adaptive thresholds. The vertical threshold is based on the greater of the 99.5th percentile or 10% of the max value, clamped between 0.015 and 0.1. The horizontal threshold scales inversely with peak amplitude to avoid false detections.

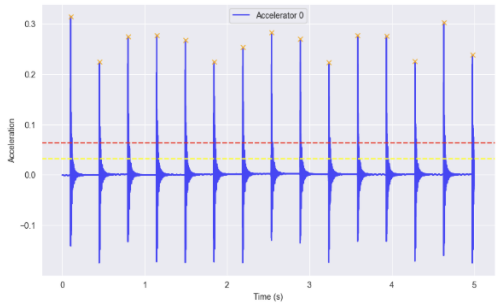

Figure 3.—Detected peaks using adaptive thresholding.

3.1.2 Derived Peak Features

From each run, the following are calculated:

- Number of statistically significant dominant rhythms
- Mean, median, and standard deviation of peak-to-peak intervals
- Peak magnitude statistics (max, median, std)
- Peaks per second
- Sum of peak magnitudes per second

The algorithm for detecting the number of statistically significant dominant rhythms is detailed in Appendix A.

3.1.3 Additional Metrics

The following metrics are included:

- Percent of time above threshold
- Global signal standard deviation

3.2 Frequency Domain Features

3.2.1 Spectral Transformation

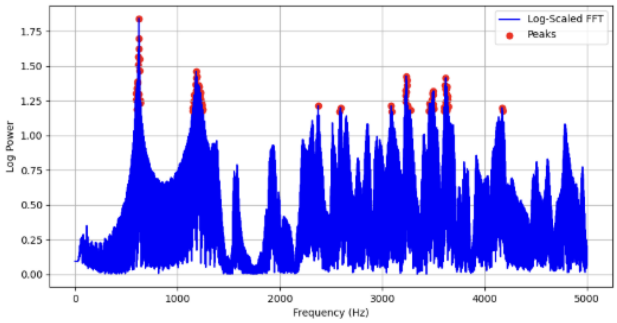

Figure 4.—FFT of filtered accelerometer signal.

A high-pass Butterworth filter is applied, followed by FFT and Welch's method to compute spectral features, as seen in Figure 4.

3.2.2 Extracted Features

- Dominant frequency
- Number of spectral peaks
- Weighted average frequency
- Mean and standard deviation of spectral power
- Spectral entropy

4 Unsupervised Learning

4.1 Pipeline

An unsupervised learning pipeline is implemented to analyze acoustic boiling regime data. The pipeline consists of the following steps:

- **Feature Standardization:** All extracted features are standardized using `StandardScaler` to ensure each feature contributes equally to the analysis.

- **Dimensionality Reduction:** Principal Component Analysis (PCA) is applied to the standardized features. The first 10 principal components are retained, capturing approximately 97% of the total variance in the dataset. This reduces noise and highlights the most informative patterns. *(See Figure 5 for the scree plot, which shows the cumulative variance explained by varying numbers of principal components.)*

- **Clustering:** KMeans clustering is performed in the reduced PCA space, enabling the identification of natural groupings and patterns within the data without relying on labels.

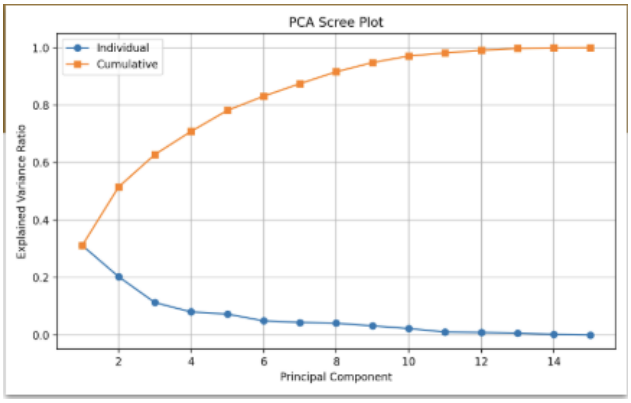

Figure 5.—Scree plot of PCA variance.

4.2 Cluster Analysis

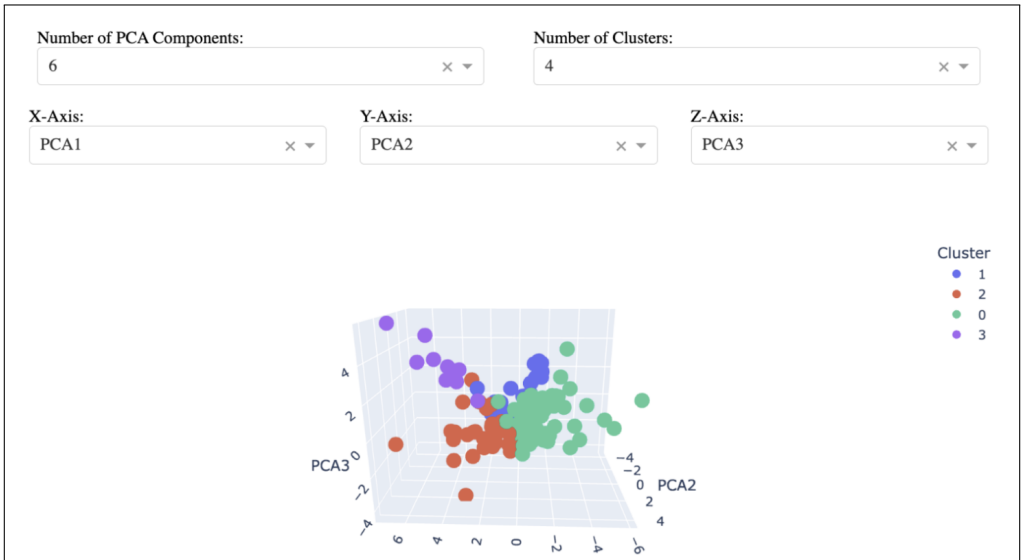

Figure 6.—PCA projection of clustered experiments.

Varying k revealed distinct groupings, interpreted using PCA loadings and rhythm patterns. Figure 6 displays the data plotted in the PCA space, with k-means clustering applied with $k = 4$.

4.3 Cluster Validation

To assess clustering quality and interpret cluster meanings, the Szymkiewicz–Simpson overlap is computed between each cluster and true class:

$$\mathrm{Sim}(A, B) = \frac{|A \cap B|}{\min(|A|, |B|)}$$

Values close to 1 indicate a strong match between a cluster and a class, whereas values near 0 suggest little to no overlap.

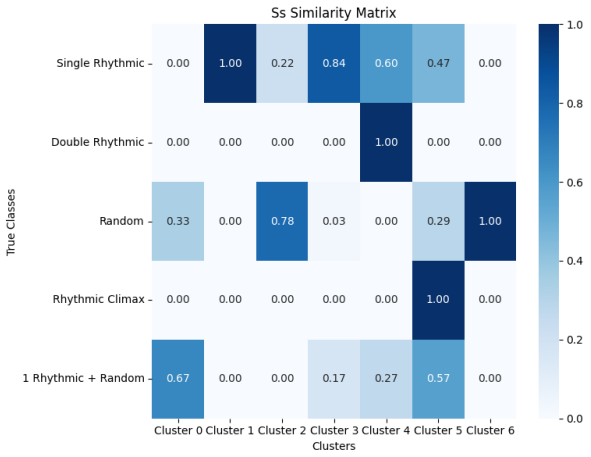

Figure 7.—Cluster validation using Szymkiewicz–Simpson overlap coefficient.

Figure 7 presents the resulting overlap matrix with 7 clusters.

5 Supervised Learning

5.1 Training and Evaluation

The supervised learning stage of the pipeline leverages labeled data to train a Decision Tree classifier for boiling regime classification. After feature extraction, categorical labels are encoded and the data is split into training and validation folds. Cross-validation is used to provide robust estimates of model performance.

Model training and evaluation are fully automated: the decision tree is fit on the training data, and predictions are generated for each fold. Performance metrics, including per-class F1-scores and a weighted F1-score, are computed to assess classification accuracy across both dominant and minority classes. The pipeline also generates visualizations such as feature importance plots and confusion matrices, which are saved for downstream analysis and reporting.

This approach ensures that model evaluation is consistent, transparent, and easily extensible to new data.

5.2 Results

Table 1.—F1-scores by class from Decision Tree classifier

Class	**F1-score (%)**
Single Rhythmic	85.2
Random	83.4
Noise	87.4
Rare Classes	Low due to insufficient support
Weighted F1-score	**79.1**

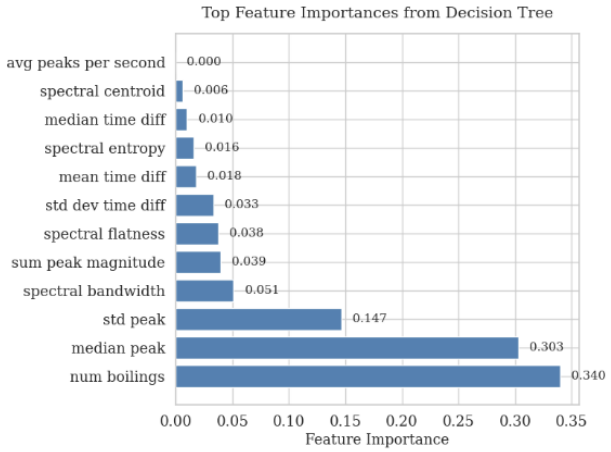

Figure 8.—Feature importance from decision tree.

As shown in Figure 8, the most influential features identified by the decision tree include the number of boilings, which captures the frequency of boiling events; the median and standard deviation of peak magnitudes, which reflect the central tendency and variability of acoustic signal intensity and the spectral bandwidth, which characterizes the distribution of energy across the frequency domain. These features collectively provide a robust representation of both temporal and spectral characteristics relevant to boiling regime classification.

5.3 Comparison with Other Methods

Alternative modeling approaches, such as XGBoost and neural networks, were also explored for boiling regime classification. However, these models consistently underperformed when compared to the Decision Tree classifier. Across both dominant and minority classes, they yielded lower F1-scores and failed to identify meaningful distinctions among rhythmic patterns. Moreover, their lack of interpretability limited the ability to extract actionable insights or visualize decision boundaries—a key requirement for this domain. In contrast, the Decision Tree offered a reliable and transparent solution, aligning well with the interpretability demands and data limitations of this study.

5.4 Handling Class Imbalance

Several techniques were evaluated to address the imbalance in class distribution, including class weighting, random oversampling, and Synthetic Minority Over-sampling Technique (SMOTE). Despite these efforts, improvements remained modest due to the severe sparsity in certain labels. Minority classes such as *Double Rhythmic* and *Rhythmic Climax* were especially affected, with insufficient samples to enable generalizable learning. These limitations suggest that future progress may depend more on collecting targeted additional data or employing domain-informed data augmentation techniques to enrich underrepresented classes.

5.5 Confusion Matrix Analysis

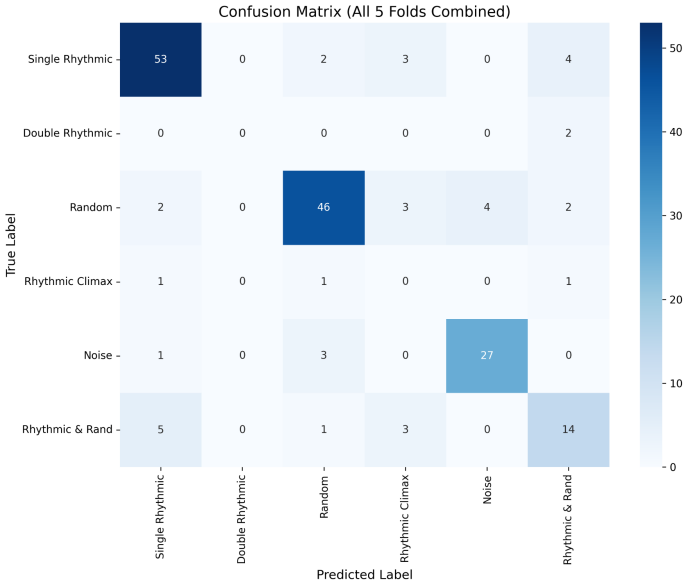

Figure 9.—Confusion matrix.

Figure 9 presents the confusion matrix aggregated across all five folds of cross-validation. Most misclassifications occurred between acoustically or structurally similar boiling regimes. Notably:

- *Single Rhythmic* was occasionally misclassified as *Rhythmic Climax* or *Rhythmic & Random*.
- *Random* sometimes overlapped with both *Noise* and *Rhythmic Climax*.
- *Double Rhythmic* and *Rhythmic Climax* classes yielded very low true positive rates, reinforcing the issue of class sparsity.

These trends suggest that while the model is effective at detecting dominant rhythmic structures, it struggles to separate closely related or infrequent patterns. This difficulty likely stems from overlapping feature representations and limited training data for the minority classes.

6 Web Application for Interactive Exploration and Classification

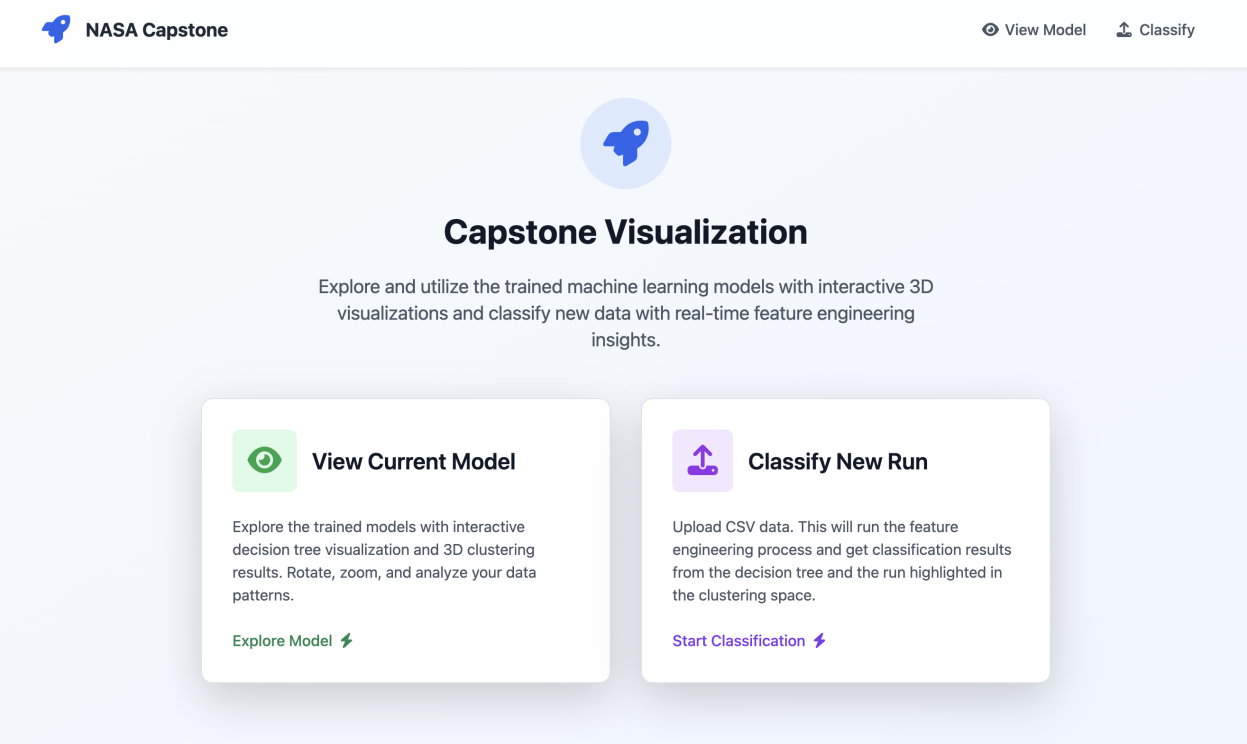

Figure 10.—Web app landing page presenting two primary modes: model exploration and new run classification.

To bridge the gap between model development and researcher usability, an interactive web application was built using Dash, as seen in Figure 10. This web interface serves as both an analytical and interpretive tool, enabling researchers at NASA to explore clustering results, visualize decision boundaries, and classify new experimental runs with minimal technical overhead.

The application supports two primary modes of use:

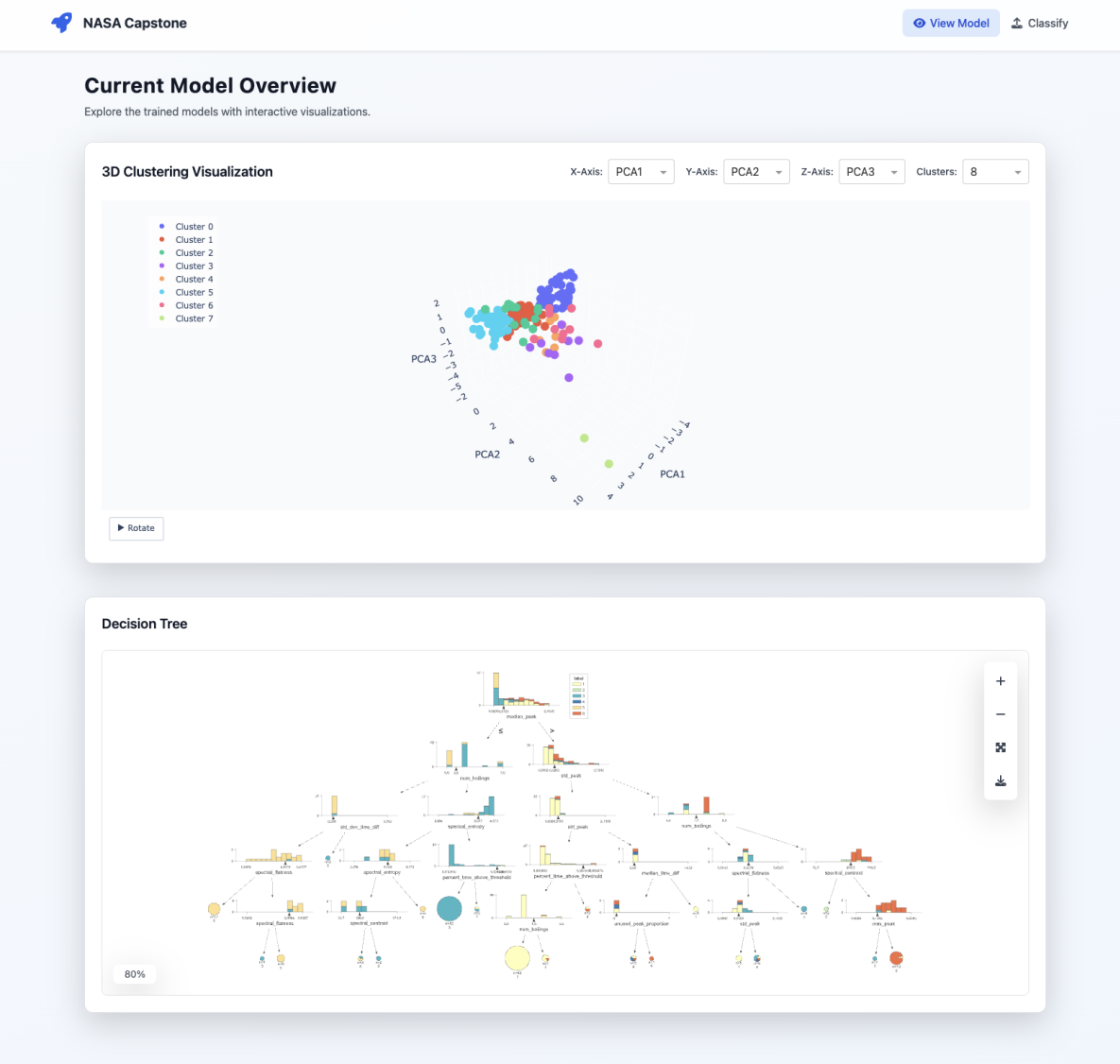

Figure 11.—Model Exploration mode.

1. **Model Exploration Mode (Figure 11):** The behavior of the current trained unsupervised and supervised models can be inspected. This includes an interpretable decision tree visualization rendered as a zoomable, pannable SVG, allowing users to trace the logical flow of predictions and understand how specific features influence model decisions. In parallel, clustering results can be explored in a 3D PCA-reduced space. The number of clusters and selected PCA axes can be dynamically adjusted to reveal latent structure in the data and identify potential regime separability.

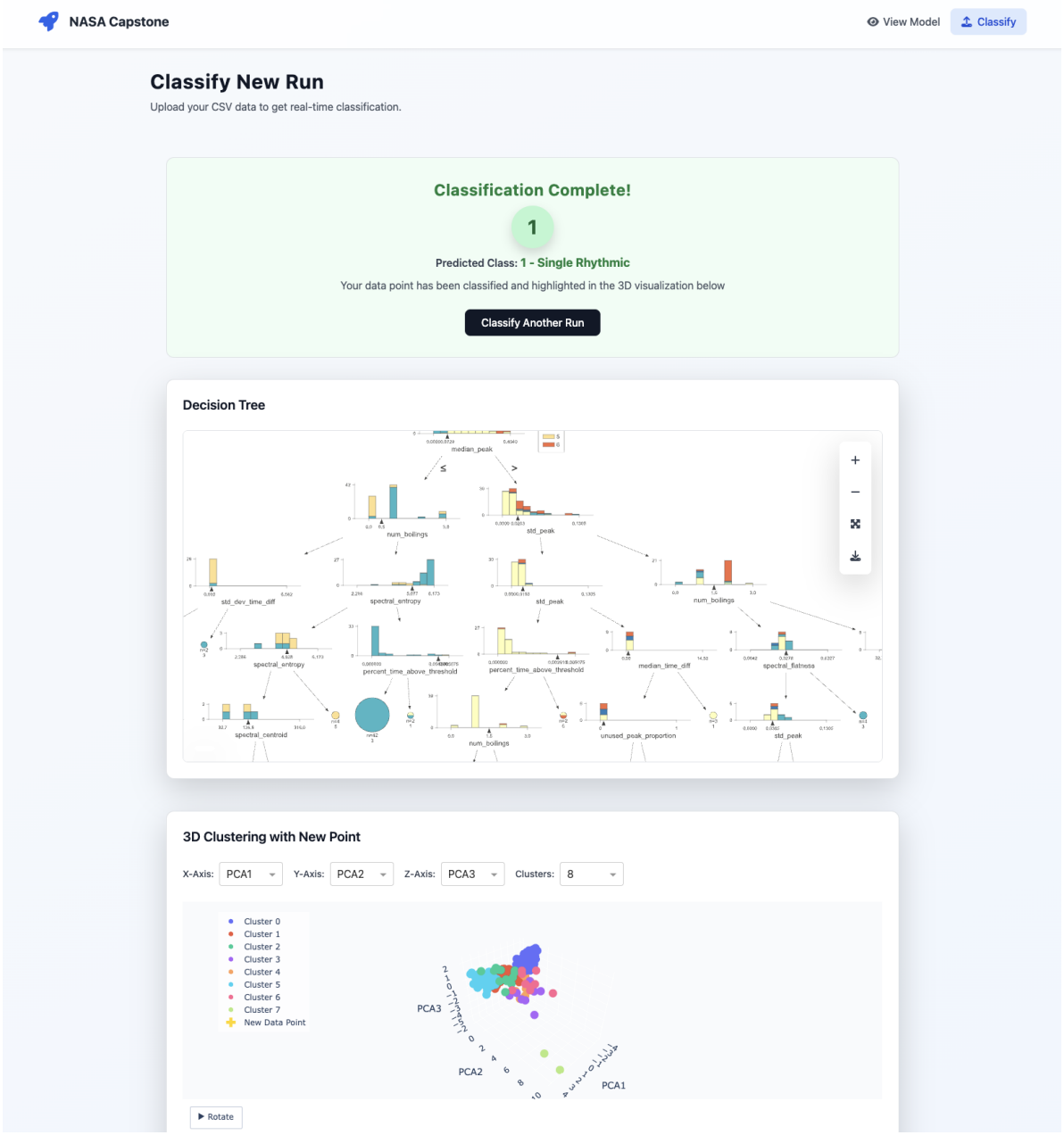

Figure 12.—Classification mode output: predicted boiling regime and projection of the new data point in PCA cluster space.

2. **Classification Mode (Figure 12):** New experimental runs can be uploaded in a CSV format. Once uploaded, the application automatically applies the full feature engineering pipeline, including time-domain and frequency-domain transformations. The extracted features are passed through the trained decision tree classifier, which outputs a predicted boiling regime, class probabilities, and a list of influential features. Simultaneously, the new run is projected into the PCA space and overlaid on the existing cluster visualization. This

dual approach allows classification outcomes to be assessed in both a supervised context (via the decision tree) and an unsupervised context (via clustering), offering a more holistic understanding of the run's regime.

Together, these capabilities transform the machine learning pipeline into a robust, real-time decision support tool. The web application enables interactive exploration of both the unsupervised (clustering) and supervised (decision tree) models, validation of predictions, and interpretation of key signal characteristics driving boiling regime classification. Additionally, the modular architecture of the codebase supports future extensions and modifications, whether to the regimes, experimental runs, decision tree logic, or clustering pipeline. This flexibility enables potential integrations such as onboard deployment with spacecraft sensor streams or adaptive model retraining as new data becomes available.

7 Conclusion

A machine learning pipeline for detecting early-stage boiling in cryogenic fuel systems using high-resolution acoustic emissions is presented. The approach leverages both time- and frequency-domain signal processing to extract responsive boiling indicators. These features feed into a hybrid modeling framework consisting of unsupervised clustering for regime discovery and supervised decision tree classification for real-time interpretability and classification.

To support deployment and usability in practical research settings, a custom web application was developed to visualize model behavior, inspect boiling regime boundaries, and classify new experimental runs. This interface bridges the gap between data science and application, making advanced analytics accessible and actionable.

The results demonstrate that acoustic-based detection, when paired with machine learning, offers a viable path forward for enhancing safety and situational awareness in cryogenic systems. The modular and extensible design of the pipeline also enables ongoing adaptation, supporting future extensions such as retraining with new data or expansion to other discovered regimes. Ultimately, this work lays the foundation for building safer, smarter, and more autonomous cryogenic fuel monitoring systems for future space missions.

Appendix A Detection of Dominant Rhythmic Patterns Algorithm

Purpose

This algorithm aims to detect recurring rhythmic patterns in a sequence of detected acoustic peaks. It evaluates every possible candidate interval derived from peak differences, tests each rhythm statistically, and consolidates similar patterns while removing weak or redundant ones. The result is a clean list of dominant intervals that likely represent true underlying rhythmic structure in the data.

Plain English Overview of Algorithm

0. **Estimate Noise Level**
   Before any rhythm analysis, the algorithm estimates the natural variability in peak timing and amplitude. This standard deviation is used to compute a margin of tolerance when evaluating rhythmic alignment and to calibrate statistical tests later in the process.

1. **Generate Rhythm Candidates**
   Every pair of peaks is used to define a potential rhythm interval $d = x_j - x_i$, anchored at x_i. Only differences that allow a sufficient number of repetitions (typically based on $\sqrt{n}$) within the signal duration are retained.

2. **Count Hits Per Candidate**
   For each candidate, the algorithm walks forward in time from the anchor using $t_k = \text{anchor} + k \cdot d$, checking whether predicted steps align closely with real peaks, both in the x and y direction. Each match is a "hit," and both the number of hits and total prediction attempts (tries) are recorded.

3. **Prune Candidates via Binomial Test**
   The algorithm tests each candidate using a one-sided binomial hypothesis test. It asks: "Is the observed hit rate significantly better than random chance?" Candidates that fail this test (after adjusting for multiple comparisons) are removed.

4. **Group Similar Candidates**
   Candidates that share a large number of overlapping hits are grouped using a similarity metric (Szymkiewicz–Simpson coefficient). Within each group, the strongest candidate is retained and others are marked as absorbed.

5. **Final Filtering by Support**
   As a final step, candidates that don't have enough total support (from both their own hits and absorbed ones) are removed. This ensures the algorithm outputs only the most robust rhythmic patterns.

The pseudocode for the algorithm is presented in Algorithm 1.

Input: sorted peak times $x = [x_1, \ldots, x_n]$, amplitudes $y = [y_1, \ldots, y_n]$, total duration T
Output: filtered list of dominant rhythmic candidates
Step 0: Estimate Noise Level;
$\sigma_x \leftarrow$ `estimate_std`(x); `// timing variability`
$\sigma_y \leftarrow$ `estimate_std`(y); `// amplitude variability`
$m_x \leftarrow z_\alpha \sigma_x$,;
$m_y \leftarrow z_\alpha \sigma_y$;
$p_{\text{null}} \leftarrow \min\left(1, \frac{2m_x n}{T}\right)$;
Step 1: Generate Rhythm Candidates;
for $i \leftarrow 1$ **to** $n-1$ **do** `// pairwise peak spacings`
  for $j \leftarrow i+1$ **to** n **do**
    $d \leftarrow x_j - x_i$;
    if $x_j + \sqrt{n}\, d > T + m_x$ **then**
    end
    else
      add candidate (d, x_i) to list;
    end
  end
end
Step 1: Generate Rhythm Candidates;
for $i \leftarrow 1$ **to** $n-1$ **do** `// pairwise peak spacings`
  for $j \leftarrow i+1$ **to** n **do**
    $d \leftarrow x_j - x_i$;
    if $x_j + \sqrt{n}\, d > T + m_x$ **then**
    end
    add candidate (d, x_i) to list;
  end
end
Step 2: Count Hits Per Candidate;
for *each candidate* (d, a) *in list* **do**
  for $k \leftarrow 0$ **to** $\lfloor (T-a)/d \rfloor$ **do**
    $t_k \leftarrow a + kd$;
    estimate $\bar{y}_k$;
    if $\exists\, x_i \in [t_k \pm m_x]$ ***and*** $y_i \in [\bar{y}_k \pm m_y]$ **then**
      hit++;
    end
    tries++;
  end
end
Step 3: Prune via Binomial Test;
for *each candidate with* h *hits and* t *tries* **do**
  $\alpha' \leftarrow \alpha / R$;
  $p \leftarrow$ `BinomialTest`$(h-2, t-2, p_{\text{null}})$;
  if $h < \sqrt{n}$ ***or*** $p \geq \alpha'$ **then**
    remove candidate;
  end
end
Step 4: Group Similar Candidates;
build similarity graph (edge if Szymkiewicz–Simpson $\geq \tau$);
for *each connected component* **do**
  keep candidate with highest centrality;
  absorb unique hits from others;
end
Step 5: Final Filtering by Support;
for *each remaining candidate* **do**
  if *hits + absorbed* $< \sqrt{n}$ **then**
    remove candidate;
  end
end
return remaining candidates as dominant rhythmic intervals;

Algorithm 1: Detection of Dominant Rhythmic Patterns in Acoustic Peaks

Example Walkthrough Using Peak Time Array

We demonstrate the full algorithm using the following observed peak times from an acoustic signal:

$$\text{peaks} = \left\{ \begin{array}{llll} 0.1035, & 0.3391, & 0.5746, & 0.8100, \\ 1.0454, & 1.2791, & 1.5160, & 1.7496, \\ 1.9866, & 2.2220, & 2.4574, & 2.6930, \\ 2.9286, & 3.1641, & 3.3999, & 3.6359, \\ 3.8722, & 4.1088, & 4.3458, & 4.5828, \\ 4.8197 & & & \end{array} \right\}$$

The following plot shows the original acoustic signal, with peaks marked:

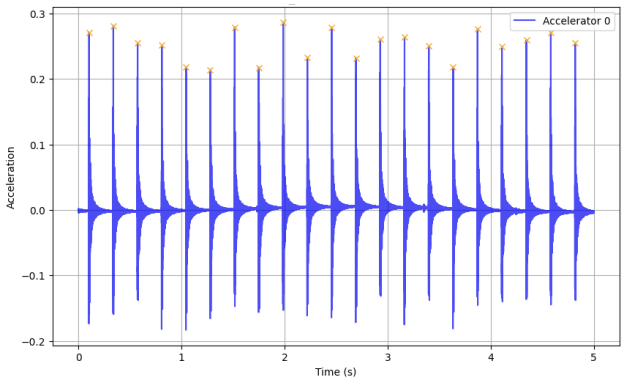

Figure 13.—Acoustic signal with extracted peaks.

Step 0: Estimate Noise Level

We calculate the global standard deviation of peak-to-peak spacing:

$$\text{SD} = 0.00091 \quad \Rightarrow \quad \text{Margin} = z \cdot \text{SD} = 0.0015$$

The probability of a random hit in a margin window is estimated as:

$$p_{\text{null}} = \frac{2 \cdot \text{margin} \cdot \#\text{peaks}}{\text{run length}} = \frac{2 \cdot 0.0015 \cdot 21}{5} \approx 0.0126$$

Step 1: Generate Rhythm Candidates

For each peak pair (i, j), we compute the difference $d = x_j - x_i$ and retain it as a candidate if it allows at least $\sqrt{n}$ steps within the duration.

Example early candidates:

- Candidate 0: $d = 0.2356$, anchor $= 0.1035$
- Candidate 1: $d = 0.4711$, anchor $= 0.1035$
- Candidate 2: $d = 0.7065$, anchor $= 0.1035$

This process generates a total of 41 candidates.

Step 2: Count Hits Per Candidate

We count how many predicted steps align with real peaks (within the x and y margin), starting from each candidate's anchor and incrementing by d. The first two hits (anchor and anchor+d) are assumed, and only later steps are evaluated.

Candidate ID	d (sec)	Anchor	Hits	Tries
0	0.2356	0.1035	20	20
1	0.4711	0.1035	10	10
2	0.7065	0.1035	6	6
3	0.9429	0.1035	5	5
4	1.1785	0.1035	3	4

Step 3: Prune Candidates via Binomial Test

Each candidate is evaluated using a one-sided binomial test under:

$$H_0 : \text{hit rate} = p_{\text{null}} \qquad H_A : \text{hit rate} > p_{\text{null}}$$

A Bonferroni adjustment is applied using α/R for R candidates. Clusters failing the test are removed.

Step 4: Group Similar Candidates

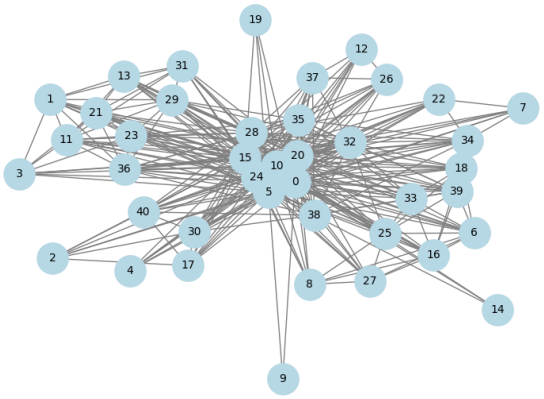

Figure 14.—Candidate similarity graph.

Remaining candidates are grouped based on the Szymkiewicz–Simpson overlap of their hit indices:

$$\text{Sim}(A, B) = \frac{|A \cap B|}{\min(|A|, |B|)}$$

Note that $0 \leq \text{Sim}(A, B) \leq 1$, where a value of 0 indicates that the sets are disjoint, and a value of 1 indicates that the smaller set is entirely contained within the larger. To identify and consolidate redundant candidates, a similarity graph is constructed by connecting pairs of

candidates whose overlap exceeds a predefined threshold (e.g., 0.8). Each edge represents significant shared alignment between two candidates. Within each connected component of this graph, the candidate with the highest degree centrality is selected as the representative rhythm. All other candidates in the component are considered redundant and are absorbed into the dominant one, contributing their supporting peak hits.

Step 5: Final Filtering by Support

Candidates with too few total hits (direct + absorbed) are removed. In this example, only rhythms with $\geq \sqrt{21} \approx 5$ hits are retained.

Final Result

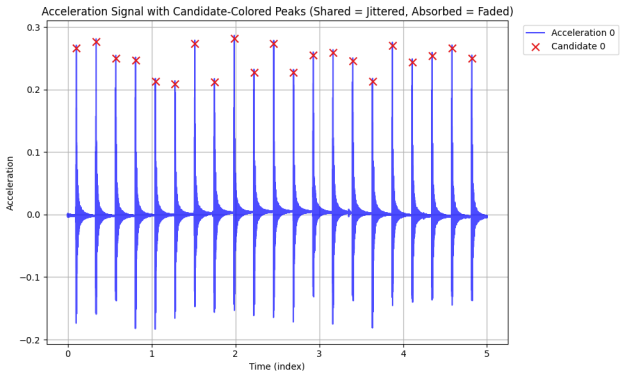

Figure 15.—Labeled acoustic signal with candidate assignments.

The final output is the strongest rhythmic regime:

Detected Rhythm: ID = 0, $\mu = 0.2356$ seconds, aligned with 20 out of 20 peaks

This rhythm is statistically significant, and it absorbs several weaker candidates into a unified regime.

The figure below shows the acoustic signal with peaks labeled according to their assigned rhythmic candidate. Each candidate is represented by a distinct color—if multiple rhythmic candidates are present, the peaks associated with each are shown in different colors.

Example on Double Rhythmic Signal

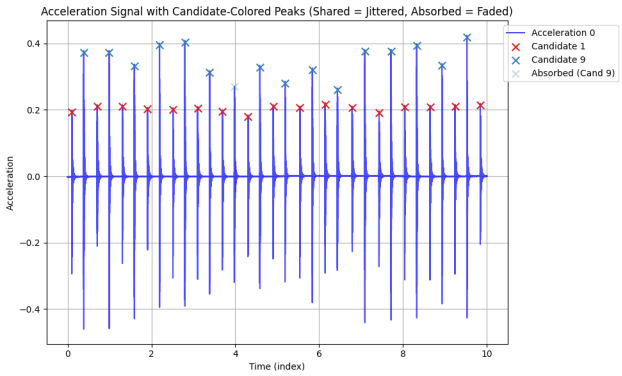

Figure 16.—Labeled double rhythmic acoustic signal with candidate assignments.

Figure 17.—Double rhythmic similarity graph.

We also illustrate the algorithm on a run classified as double rhythmic in Figure 16. The similarity graph is shown in Figure 17. Each of the two distinct connected components corresponds to one of the two rhythms, as expected.

Notes

- Peaks that align with a candidate's predicted steps—but were not part of its original cluster—are marked as absorbed, as seen in Figure 16.
- Absorbed peaks are visualized using a lighter shade of the candidate's color to distinguish them from originally clustered peaks.
- Peaks not matched to any candidate rhythm are considered unused and are displayed in gray and likely correspond to random boiling. A higher proportion of unused peaks may indicate random boilings.

Appendix B Clustering Interpretation and Principal Components

B.1 Overview

This appendix presents a sample clustering outcome from our web application, using three principal components (PC1, PC2, PC3) and grouping the data into three clusters. The figure below visualizes each experimental run in 3D space, with colors indicating cluster assignments.

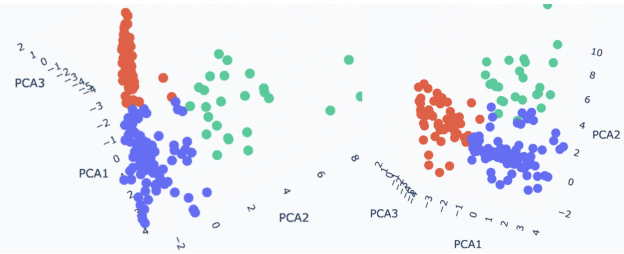

Figure 18.—3D projection of boiling experiments clustered by PCA components.

B.2 PCA Loadings and Cluster Interpretation

Principal Component Analysis (PCA) was used to reduce the complex, multi-dimensional feature space into a few principal axes that capture the dominant patterns in the boiling regime data. By examining the contributions of each original feature to the principal components, we can interpret the underlying physical and statistical characteristics that differentiate the data.

Principal Component 1 (PCA1):

The first principal component primarily reflects the overall intensity and activity of the boiling signal. High values along this axis correspond to runs with more frequent and larger acoustic events, as well as signals that are more complex and less uniform. In contrast, lower values indicate quieter runs with fewer, smaller, or more uniform events, and a more regular or "flat" signal profile.

Principal Component 2 (PCA2):

The second principal component is most influenced by the temporal structure of the boiling events and the presence of unused or less prominent acoustic features. High values along this axis are associated with runs where the timing between events is more variable or extended, and where a greater proportion of potential events are not strongly expressed in the signal. This suggests a regime with more irregular or sporadic boiling activity.

Principal Component 3 (PCA3):

The third principal component captures variation related to the complexity and distribution of energy within the signal. High values along this axis are associated with runs where the acoustic energy is more broadly distributed across different frequencies and where the signal exhibits greater unpredictability or irregularity. This suggests that PCA3 distinguishes between boiling regimes with more complex, less periodic acoustic patterns and those with simpler, more predictable structures.

Cluster Interpretation in PCA Space:

- **Cluster 0 (green):** This group is distinguished by higher values along the second principal component, indicating runs with more irregular timing between events and a greater presence of subtle or less pronounced acoustic activity.
- **Cluster 1 (blue):** This cluster stands out for its higher values along the first principal component, representing runs with more intense, frequent, and complex boiling activity.
- **Cluster 2 (red):** This group is characterized by lower values along the first principal component, corresponding to runs with less intense, more uniform, and quieter boiling signals.

This analysis shows that the main axes of variation in the data correspond to differences in both the intensity and regularity of boiling activity, as well as the presence of subtle or sporadic events. The clustering in PCA space thus provides a physically meaningful separation of boiling regimes, reflecting both the strength and the temporal structure of the acoustic signals.

Appendix C Decision Tree Summary and Metrics

C.1 Trained Decision Tree

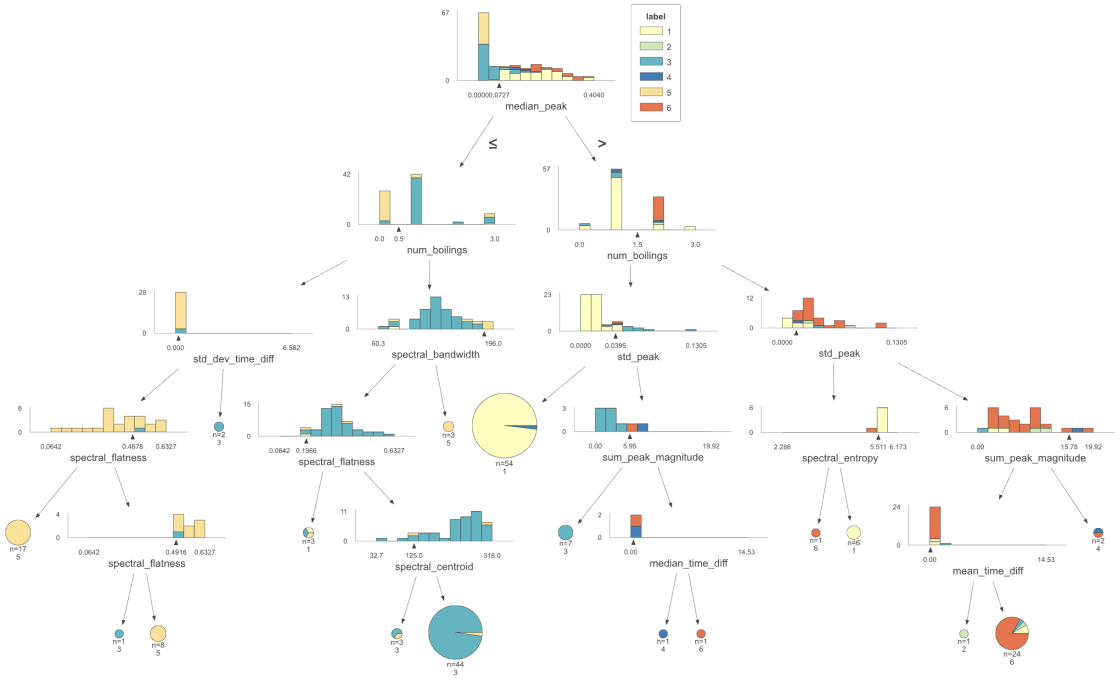

Figure 19.—Final decision tree trained on acoustic feature set.

Figure 19 shows our final trained decision tree. This model was constrained to a maximum depth of five to improve interpretability and prevent overfitting.

Table 2.—Decision Tree Classification Report

Class	Support	Precision	Recall	F1-Score
Single Rhythmic	62	86.56	85.48	85.22
Double Rhythmic	2	0.00	0.00	0.00
Random	57	87.54	80.70	83.36
Rhythmic Climax	3	0.00	0.00	0.00
Noise	31	90.16	87.09	87.38
Rhythmic & Rand	23	68.98	60.86	58.11
Weighted Avg	**178**	**82.80**	**78.65**	**79.11**

C.2 Interpretation

The decision tree performed well for high-support classes, achieving F1-scores above 83% for Single Rhythmic, Random, and Noise. However, the model struggled with underrepresented classes (Double Rhythmic, Rhythmic Climax), resulting in F1-scores of zero due to insufficient training data. These results underscore the need for class-balancing techniques and possibly more data or ensemble methods to boost performance on rare classes.

References

1. C. Dunlap, H. Pandey, E. Weems, and H. Hu, "Nonintrusive heat flux quantification using acoustic emissions during pool boiling," *Applied Thermal Engineering*, vol. 228, 2023, Art. no. 120558.

2. S. Barathula and K. Srinivasan, "Review on research progress in boiling acoustics," *International Communications in Heat and Mass Transfer*, vol. 139, 2022, Art. no. 106465.

3. J. Tang, G. Xie, J. Bao, Z. Mo, H. Liu, and M. Du, "Experimental study of sound emission in subcooled pool boiling on a small heating surface," *Chemical Engineering Science*, vol. 188, pp. 179–191, 2018.

4. B. M. Dorofeev and V. I. Volkova, "An acoustic method of investigation of the process of boiling," *High Temperature*, vol. 43, no. 4, pp. 620–627, 2005.

5. B. M. Dorofeev and V. I. Volkova, "The effect of evaporation and condensation in vapor bubbles on the hydrodynamic sound generation in a subcooled boiling liquid," *Acoustical Physics*, vol. 52, no. 2, pp. 173–179, 2006.

6. Y. Ueki and K. Ara, "Proof of concept of acoustic detection of boiling inception and state transition using deep neural network," *International Communications in Heat and Mass Transfer*, vol. 129, 2021, Art. no. 105675.

7. V. K. Dhir, "Boiling under microgravity conditions," in *Proc. 12th Int. Heat Transfer Conf.*, Grenoble, France, 2002.

8. C. B. Muratov, V. V. Osipov, and V. N. Smelyanskiy, "Issues of long-term cryogenic propellant storage in microgravity," NASA Technical Memorandum TM-2011-215988, ARC-E-DAA-TN4295, 2011.

9. M. Hasan and R. Balasubramaniam, "Analysis of the pressure rise in a partially filled liquid tank in microgravity with low wall heat flux and simultaneous boiling and condensation," in *50th AIAA Aerospace Sciences Meeting*, 2012.